Magnetohydrodynamic Flow in the Inlet Region of a Straight Channel

A. BRANDT AND J. GILLIS
Department of Applied Mathematics, Weizmann Institute of Science, Rehovoth, Israel
(Received 12 August 1965; final manuscript received 22 November 1965)

The flow is considered of an incompressible conducting viscous fluid in the inlet region of a straight channel in the presence of a transverse magnetic field. The complete equations are solved numerically without any approximating assumptions. Various characteristics of the flow and their dependence on the physical parameters are deduced. Values of Reynolds number up to 500 are considered. Velocity profiles near the inlet are found to have points of inflection. The distance to the terminal regime is studied, and the results, in the limiting case of large Reynolds number, compared with those of other workers. The boundary layer thickness is found to be proportional to x^{α} (for a small range of x) where $\alpha \approx 1.2$ at zero Reynolds number and decreases to 0.5 as the Reynolds number increases. The exact pressure distribution is also obtained.

I. INTRODUCTION

THE central purpose of this work is to develop methods for the numerical solution of the equations of magnetohydrodynamics. As a special case, i.e., when the magnetic field is zero, we have dealt also with the Navier–Stokes equations. The general approach has been through specific problems, but it will be seen that the methods are of more general application.

We have confined our attention to two-dimensional steady state flows of incompressible homogeneous viscous liquids at finite values of R, R_m, the Reynolds number and magnetic Reynolds number, respectively. This paper deals with the flow in the inlet region of a straight channel where the magnetic field, if any, is transverse. We have also considered certain modifications of the boundary, and the results of applying our methods to these modified problems will be described elsewhere.

In Sec. II we present a detailed derivation of the governing equations and boundary conditions. The method of solution is described in Sec. III as also some of the methods used for attaining the desired accuracy. Some methods for checking the accuracy are given in Sec. IV.

The numerical results obtained for a straight channel are presented in Sec. V, and where possible, we have compared our results with those obtained by other workers.

II. FORMULATION OF PROBLEM

(a) The Differential Equations

Our starting point will be the steady-state magnetohydrodynamic equations (in rationalized mks units),

$$(\mathbf{u}\cdot\nabla)\mathbf{u} = -\rho^{-1}\nabla p + \nabla\phi + \nu\nabla^2\mathbf{u} + \rho^{-1}\mathbf{J}\times\mathbf{B}, \quad (2.1)$$

$$\mathbf{J} = \sigma(\mathbf{E} + \mathbf{u}\times\mathbf{B}), \quad (2.2)$$

$$\nabla\times\mathbf{B} = \mu\mathbf{J}, \quad (2.3)$$

$$\nabla\times\mathbf{E} = -\partial\mathbf{B}/\partial t = 0, \quad (2.4)$$

$$\text{div}\,\mathbf{u} = 0, \quad (2.5)$$

$$\text{div}\,\mathbf{B} = 0. \quad (2.6)$$

In these equations ρ represents the fluid density, ν its kinematic viscosity, μ its magnetic permeability, and σ its electrical conductivity, all assumed constant. Of the dependent variables, $\mathbf{u}$ represents the fluid velocity, $\mathbf{B}$ the total magnetic induction, $\mathbf{J}$ the electrical current density, $\mathbf{E}$ the electrostatic force field, p the pressure, and ϕ the potential of any external force field which may be present.

To simplify the subsequent notation we take coordinate axes $0x_1$, $0x_2$, $0x_3$, with $0x_3$ perpendicular to the plane of our two-dimensional flow. In general, we denote the components of any vector $\mathbf{q}$ by (q_1, q_2, q_3). To be precise, our assumption of two-dimensional steady-state flow is expressed by the fact that none of the components of $\mathbf{u}$, $\mathbf{E}$, $\mathbf{B}$, or $\mathbf{J}$ depend on either x_3 or t. It follows then from (2.5), (2.6) that we can find two scalar functions $\psi(x_1, x_2)$, $\beta(x_1, x_2)$ such that

$$u_1 = \partial\psi/\partial x_2, \qquad u_2 = -\partial\psi/\partial x_1,$$
$$B_1 = \partial\beta/\partial x_2, \qquad B_2 = -\partial\beta/\partial x_1. \quad (2.7)$$

We see in the usual way from (2.4) that

$$\partial E_3/\partial x_1 = \partial E_3/\partial x_2 = 0, \quad (2.8)$$

and so E_3 is a constant. Now take the curl of both sides of (2.1), making use of (2.3), (2.7). The x_3-component yields

$$\partial(\psi, \nabla^2\psi)/\partial(x_1, x_2) = -\nu\nabla^4\psi + (1/\rho\mu)[\partial(\beta, \nabla^2\beta)/\partial(x_1, x_2)]. \quad (2.9)$$

Again, we see from (2.2), (2.3) that

$$\sigma\{E_3 + [\partial(\psi, \beta)/\partial(x_1, x_2)]\} = J_3 = -\mu^{-1} \nabla^2\beta. \tag{2.10}$$

The equations (2.9), (2.10) are to determine the functions ψ, β. The constant E_3 is determined by the boundary conditions.

(b) Boundary Conditions

We define the channel by $-a \leq x_2 \leq a$, $x_1 \geq 0$, with the inlet at $x = 0$. The boundary conditions are

$$u_1(x_1, \pm a) = u_2(x_1, \pm a) = 0 \text{ for } x_1 > 0, \tag{2.11}$$

$$u_1(0, x_2) = \text{const } [= U \text{ (say)}], \tag{2.12}$$

$$u_2(0, x_2) = 0, \tag{2.13}$$

$$B_1(0, x_2) = 0, \tag{2.14}$$

$$B_2(x_1, \pm a) = b \text{ (const)}. \tag{2.15}$$

These express what is physically assumed about the fluid velocity vector and normal components of magnetic induction at the boundaries. In fact our method of solution would work equally well for more general boundary values of these quantities.

To make the problem determinate something must be said about the conditions at infinity in the x_1 direction. Briefly, we assume a stable and laminar flow which becomes independent of x_1 as the latter tends to $+\infty$. It is well known that the flow will then have the Hartmann pattern [see (2.25), (2.26) below].

In the special case $b = 0$, i.e., no external magnetic field, the equations simplify, in an obvious way, and the limiting flow becomes parabolic.

(c) Dimensionless Variables

We write

$$x' = x_1/a, \quad y' = x_2/a, \quad z' = x_3/a,$$
$$u = u_1/U, \quad v = u_2/U, \quad \psi' = \psi/(aU),$$
$$p' = p/(\rho U^2), \quad \mathbf{B}' = \mathbf{B}/b_0, \quad \beta' = \beta/(ab_0), \tag{2.16}$$

where

$$b_0 = a^{-1}(\nu\rho/\sigma)^{\frac{1}{2}}, \quad \mathbf{E} = \mathbf{E}/(Ub_0), \quad \mathbf{J} = \mathbf{J}/(Ub_0\sigma).$$

We now rewrite (2.9), (2.10) in the new variables, dropping the primes which were just introduced. The equations become

$$\psi_y \nabla^2\psi_x - \psi_x \nabla^2\psi_y = (2/R) \nabla^4\psi + (4/RR_m)(\beta_y \nabla^2\beta_x - \beta_x \nabla^2\beta_y), \tag{2.17}$$

$$\psi_y\beta_x - \psi_x\beta_y = E_3 + (2/R_m) \nabla^2\beta, \tag{2.18}$$

where $R = 2aU/\nu$, $R_m = 2a\mu\sigma U$, and the subscripts x, y denote differentiation.

The boundary conditions, in the new variables, are easily seen to be equivalent to

$$\psi(x, 1) = 1, \quad \psi(x, -1) = -1, \tag{2.19}$$

$$\psi_y(x, \pm 1) = 0, \tag{2.20}$$

$$\psi(0, y) = y, \tag{2.21}$$

$$\psi_x(0, y) = 0, \tag{2.22}$$

$$\beta(0, y) = 0, \tag{2.23}$$

$$\beta_x(x, \pm 1) = -M, \tag{2.24}$$

where $M = b/B_0$ (the Hartmann number). The flow pattern for large x becomes [provided $E_3 = -M$, see (d) below].

$$\psi(\infty, y) = K[y \cosh M - M^{-1} \sinh My], \tag{2.25}$$

$$\beta(x, y) \sim \tfrac{1}{2}KR_m[M^{-1} \cosh My - \tfrac{1}{2}y^2 \sinh M] - Mx, \tag{2.26}$$

where

$$K = [\cosh M - (\sinh M/M)]^{-1}.$$

(d) Indeterminancy of E_3

The above equations include the apparently undetermined constant E_3. However, in any practical case, account must be taken of the mode of closure of the electrical circuit. The description of the flow as two-dimensional is essentially equivalent to considering walls at $z = \pm K$, where K is very large. These walls may be connected through some circuit outside of the channel, or not. In the latter case the net flow of current in the z direction is zero. This, as is well known,[1] may be expressed in terms of our dimensionless variables by the condition $E_3 = -M$. In fact it is this case which forms the subject of our computed solutions though there would be no fundamental change required to adapt the methods to other cases.

(e) The Hydrodynamic Problem

For future reference it will be convenient to formulate explicitly the special case $b = 0$. The equations then become

$$\psi_y \nabla^2\psi_x - \psi_x \nabla^2\psi_y = 2R^{-1} \nabla^4\psi, \tag{2.27}$$

with the same boundary conditions on ψ as before, viz., conditions (2.19)–(2.22) together with

$$\psi(\infty, y) = \tfrac{1}{2}(3y - y^3). \tag{2.28}$$

[1] R. Hide and P. H. Roberts, in *Advances in Applied Mechanics* (Academic Press Inc., New York, 1962), pp. 216–320.

III. METHODS OF SOLUTION

(a) Finite Difference Approximation

Equations (2.17), (2.18) were replaced directly by the simplest central finite difference equations and solved by a routine relaxation procedure, taking account of the boundary conditions. We do not go into details of the process here. The solution for the hydrodynamic case ($b = 0$) has been described in detail elsewhere,[2] and the general magnetohydrodynamic problem was simply an extension of this without fundamental change.

We merely mention here that the system found most satisfactory was point-by-point relaxation. However, one modification of the simple system was found to contribute greatly to the efficiency of the procedure, namely, to allow the machine to study the entire field and to confine the operation of the relaxation procedure to those regions where the greatest changes were required at each stage. In particular, it was possible in the case of small R_m to devote most of the computing time to correcting the fluid velocity field and, only occasionally, after several such surveys, correcting the magnetic field.

We found by trial and error that for the hydrodynamic problem (i.e., in the absence of a magnetic field),

$$\omega_c = \min\,[20(8 + h\bar{R}\bar{u})^{-1}, 2] \qquad (3.1)$$

was approximately the critical coefficient of relaxation, where h is the mesh size and $\bar{u}$ the maximum velocity occurring in the field. The significance of (3.1) is that the process diverges for $\omega > \omega_c$. This value of ω_c can be justified theoretically in case the number of mesh points is large and on the assumption that steps are taken to stabilize variations of ψ in the neighborhood of the boundary. We do not go into details of the argument here except to indicate that the justification depends on the approximate linearity of the equations when ψ is near its true value and the consideration of the matrix associated with the finite difference equations [Ref. 2, p. 8, Eq. (2.1)].

When the number of mesh points is large, the optimal value of ω is very close to ω_c, and it is therefore safe to work with a coefficient slightly below the optimal. We found $\omega = 0.9\omega_c$ to give adequately rapid convergence without danger of divergence. It should be noted that ω_c as defined by (3.1) changes as the relaxation proceeds with the change of $\bar{u}$.

[2] J. Gillis and A. Brandt, Air Force European Office of Aerospace Research Scientific Report 63-73 (1964).

In the presence of a magnetic field the determination of the optimal ω was more complicated. For small values of R_m, the same value ω_c was found to be adequate. For larger R_m, ω was again modified by trial and error methods.

In this connection we would refer to an interesting paper of Kawaguti,[3] who studied flow in a closed two-dimensional region. For larger values of $h\bar{R}\bar{u}$ he found that the relaxation procedure failed to converge. This fits entirely with what we have just said since the value of ω required was considerably less than unity while Kawaguti continued to use $\omega = 1$.

(b) First Approximate Solution

It is commonplace that in relaxation processes a fortunate choice of first approximation can have a great influence on the efficiency of the method. In our problem this was found to be of decisive importance. Since the equations concerned were nonlinear, we could not a assume that the procedure would converge to the correct solution from any start. Indeed the opposite turned out to be true, and poor starting approximations did not lead to convergence at all. Considerable thought had therefore to be devoted to the determination of a good start. The general idea was always to proceed from a previously solved problem and advance by stages to the problem under discussion. At each stage we made a small change either in the boundary values or in one of the parameters and then solved the equations by relaxation, taking as first approximation the solution of the previous stage.

This method was first applied to the hydrodynamic equation (2.27) with the boundary conditions (2.19)–(2.22) and (2.28). We denote by T_ϵ the problem of solving the equation with these boundary conditions except that (2.21) is replaced by

$$\psi(0, y) = y + \tfrac{1}{2}(1 - \epsilon)(y - y^3),$$

and let us call the solution $\psi_\epsilon(x, y)$. When $\psi_\epsilon(x, y)$ has been found, we can take it as the first approximation in the relaxation solution of $T_{\epsilon+\Delta\epsilon}$ (say). Now $\epsilon = 0$ corresponds to parabolic flow throughout the region and so $\psi_0(x, y)$ is known. Starting from this we advanced by intervals of $\Delta\epsilon = 0.1$ until we had found $\psi_1(x, y)$, i.e., the solution of the problem. In fact it was not necessary at the intermediate stages to carry the relaxation procedure to final convergence.

The introduction of the magnetic field was achieved in a similar way. Having solved the prob-

[3] M. Kawaguti, J. Phys. Soc. Japan **16**, 2307 (1961).

lem with the appropriate R, for $M = 0$, we then introduced a field ϵM and again advanced ϵ by stages to $\epsilon = 1$.

It was also found possible to advance from the solution for one value of R to that for another value by similar stages.

(c) Accuracy of the Solution

A number of steps were taken to ensure an adequate level of accuracy in our relaxation solution. The computations were first carried out on a relatively coarse grid ($h = \frac{1}{10}$). After convergence the interval was halved and the relaxation procedure restarted, taking as first approximation the result of the previous convergence, with fourth-order interpolation at the new mesh points. After each refinement the relaxation was continued until the fifth significant figure of ψ was stabilized at all the points of the lattice. This process was actually executed three times so that the final solution was for a square lattice with side $h = 1/80$.

As might have been expected refinement of the lattice, at any stage, affected the solution only in the neighborhood of the singularity on the wall at the inlet. Indeed it was this which led us to modify the program as mentioned in (a) above.

Another matter that had to be determined was for what value x_∞ of x we could safely assume that (2.25), (2.26) adequately represented the flow. We did this by assuming successively increasing values for x_∞ until the flow pattern ceased to be significantly affected by further increases.

As a check on the accuracy of our results, we compared them with results obtained by other methods. This will be described below in Sec. IV. A more detailed account of the measures adopted to safeguard accuracy is given in Ref. 2.

IV. COMPARISON WITH RESULTS OBTAINED BY OTHER METHODS

Most of the results obtained by other workers in this field relate to flow at high Reynolds number and use boundary layer approximation.[4-9] As a check on our accuracy, we carried out the computations for some of the problems up to Reynolds number, $R = 500$. The results for $R = 500$ could

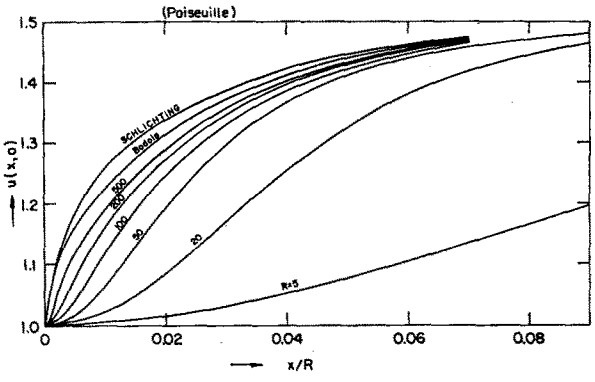

FIG. 1. Centerline velocity for various values of Reynolds number (no magnetic field). The results of Schlichting and of Bodoia and Osterle for $R \to \infty$ are shown for comparison.

be compared with the boundary layer work [see Fig. (1)]. In some cases it was convenient to extrapolate from our results to $R = \infty$ for more effective comparison with boundary layer results (see Tables I, II).

Another check was obtained by linearizing the equations and treating the flow as a perturbation of the parabolic (or Hartmann) pattern. This was of no interest for small values of x but could be expected to represent the flow reasonably well for large x. We sought to solve these linear equations by functions of the form

$$\psi(x, y) = \psi(\infty, y) + \sum_{n=1}^{\infty} A_n(y)\, e^{-\alpha_n x},$$
$$\beta(x, y) = \beta(\infty, y) + \sum_{n=1}^{\infty} B_n(y)\, e^{-\alpha_n x}. \tag{4.1}$$

Substituting this and using the boundary conditions, $B_n(\pm 1) = A_n(\pm 1) = A_n(\pm 1) = 0$, we obtained an eigenvalue equation for the α_n with smallest real part. This determined the asymptotic behavior of the flow for large x. The predictions based on this method could be compared with the relaxation solution. A fuller account of the asymptotic be-

TABLE I. Comparative values obtained for excess pressure drop for $R \to \infty$ (no magnetic field).

q	Author
0.271	Kinetic-energy end-correction
0.300	Schiller
0.313	Schlichting
0.312	Hwang and Fan
0.314	Snyder
0.315	Roidt and Cess
0.326	Sparrow, Lin, and Lundgren
0.331	Estimation from Table VII
0.338	Bodoia and Osterle
0.425	Han

[4] J. R. Bodoia and J. F. Osterle, Appl. Sci. Res. **A10**, 265 (1961).
[5] C.-L. Hwang and L.-T. Fan, Appl. Sci. Res. **B10**, 329 (1963).
[6] M. Roidt and R. D. Cess, J. Appl. Mech. **84**, 171 (1962).
[7] H. Schlichting, *Boundary Layer Theory* (McGraw-Hill Book Company, Inc., New York, 1960), 4th ed., pp. 169–171.
[8] W. T. Snyder, private communication (1964).
[9] E. M. Sparrow, S. H. Lin, and T. S. Lundgren, Phys. Fluids **7**, 338 (1964).

TABLE II. The point x_∞ where terminal régime is 97 % established, i.e., $u(\infty, 0) - u(x_\infty, 0) = 0.03\,[u(\infty, 0) - u(0, 0)]$.

R	M	R_m	X_∞	X_∞/R
0	0		1.26	
0.5	0		1.26	2.52
5	0		1.38	0.276
20	0		2.26	0.113
50	0		4.85	0.0970
100	0		9.31	0.0931
200	0		18.23	0.0912
500	0		44.8	0.0896
∞	0			0.0884
(extrapolated)				
20	0		2.26	
20	1	0.0001	2.15	
20	2	0.0001	1.90	
20	5	0.0001	1.18	
20	10	0.0001	0.78	
20	30	0.0001	0.4	
200	0		18.23	
200	1	1	17.32	
20	1	0.0001	2.151	
20	1	0.1	2.149	
20	1	1	2.131	
20	1	10	2.001	
20	1	50	1.890	
20	1	∞	1.792	

havior of the flow will be published in a subsequent paper. Suffice it to say at this stage that the agreement was satisfactory.

A further check was made possible by the analytic solution of the hydrodynamic equations for the case $R = 0$ (Stokes' flow). This has already been described in some detail (see Ref. 2, Chap. V). The agreement was within the estimated accuracy of our computation (four to five significant figures for ψ and its first partial derivatives). This check was particularly useful since that obtained from comparison with boundary layer work covered only the case of large R.

As an additional check we tried varying the finite difference formulation using higher-order approximations. The effect on the ultimate solution was very small indeed, equivalent, in fact, to one further refinement of the lattice.

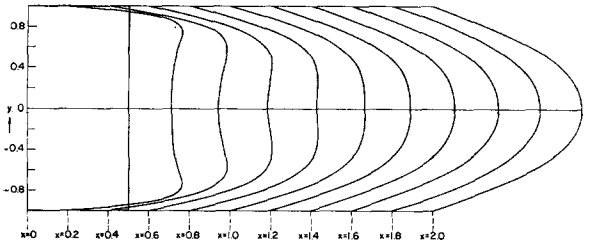

FIG. 2. Development of velocity profiles: $R = 20$, $M = 0$.

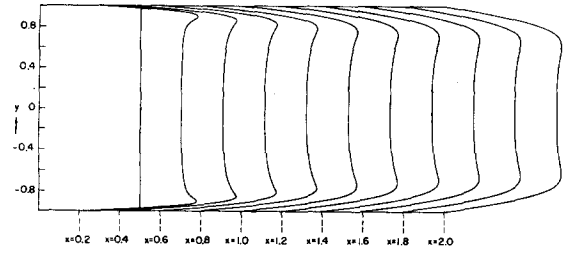

FIG. 3. Development of velocity profiles: $R = 500$, $M = 0$.

V. NUMERICAL RESULTS FOR STRAIGHT CHANNEL

(a) Velocity Profile

For large values of x the velocity profile tends to a limiting form which is parabolic in the absence of a magnetic field but which, in the presence of a magnetic field, is given by the Hartmann form

$$u = K(\cosh M - \cosh My), \qquad (5.1)$$

where M is the Hartmann number and

$$K = (\cosh M - M^{-1} \sinh M)^{-1}.$$

However, for small x the velocity profile is quite different from this and is not even convex. We give in Fig. 2 some velocity profiles for a few values of x for the case $R = 20$, $M = 0$, and in Fig. 3 profiles for $R = 500$, $M = 0$.

The presence of a magnetic field does not affect the picture in any fundamental way. In Fig. 4 we show the situation for $R = 20$, $M = 10$, $R_m = 10^{-4}$. The characteristic shape for small x includes a local minimum on the axis $y = 0$ and symmetrically situated maxima on either side of it. The physical explanation of this phenomenon is presumably that, with the slowing down of the fluid at the walls, the flow in the core must be accelerated. This effect is first felt in the vicinity of the walls, and one has to travel some distance downstream until the acceleration effect reaches the axis.

For any given x, let $y_{\max}$ $[= y_{\max}(x)]$ be the value of y for which $u(x, y)$ has its maximal value, $u_{\max}$(say), i.e.,

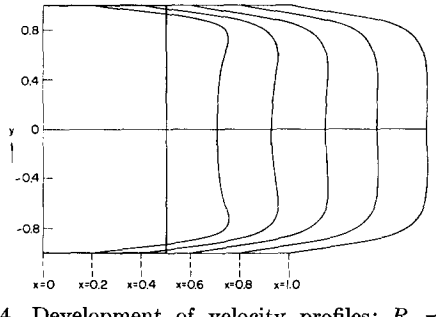

FIG. 4. Development of velocity profiles: $R = 20$, $M = 10$, $R_m = 10^{-4}$.

$$u_{\max}(x) = \max_{y} u(x, y) = u[x, y_{\max}(x)].$$

The *amplitude* of the velocity profiles is defined by

$$A_R(x) = u_{\max}(x) - u(0).$$

Let $\bar{A}(R)$ denote the greatest value of $A_R(x)$ as x varies and $\bar{x}$ the value of x at which $A_R(x) = \bar{A}(R)$. We show in Table III values of $\bar{A}$, $\bar{x}$, $y_{\max}(\bar{x})$ as functions of R in the absence of a magnetic field. Fuller details are given in Table IV.

The possible role of the point of inflection as a source of instability should be emphasized. As indicated above, the introduction of a magnetic field does not lead to any qualitative change in the behavior of the velocity profile. Indeed the magnetic lines of force also show similar behavior (see Fig. 5).

TABLE III. Amplitude of inflexion in velocity profile [see Sec. V(a)].

R	$\bar{A}$	$\bar{x}$	$y_{\max}(\bar{x})$
50	0.143	0.24	0.77
100	0.158	0.21	0.83
200	0.166	0.16	0.89
500	0.168	0.10	0.94

TABLE IV. Location and amplitude of maxima of velocity profiles.

R	x	$u(x, 0)$	$u_{\max}(x)$	$y_{\max}(x)$
0	0.05	1.00494	1.07	0.92
	0.10	1.0187	1.075	0.84
	0.15	1.0397	1.080	0.75
	0.20	1.0662	1.091	0.66
	0.25	1.0967	1.1078	0.54
	0.30	1.1296	1.1319	0.37
20	0.1	1.00553	1.105	0.86
	0.2	1.0223	1.129	0.75
	0.3	1.0494	1.149	0.65
	0.4	1.0849	1.168	0.571
	0.5	1.1258	1.1881	0.496
	0.6	1.1693	1.2098	0.421
	0.7	1.2125	1.2340	0.347
	0.8	1.2535	1.2613	0.262
	0.9	1.2911	1.2917	0.140
500	0.1	1.000770	1.169	0.94
	0.2	1.00302	1.163	0.905
	0.3	1.00659	1.156	0.879
	0.4	1.0112	1.151	0.856
	0.5	1.0166	1.148	0.836
	1.0	1.0477	1.142	0.754
	2.0	1.0998	1.151	0.64
	3.0	1.135	1.168	0.55
	4.0	1.162	1.189	0.48
	6.0	1.211	1.223	0.37
	8.0	1.252	1.256	0.26
	10.0	1.2879	1.2882	0.13

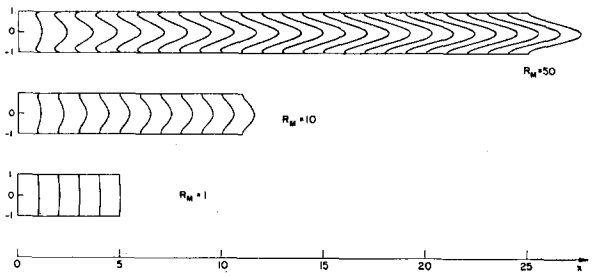

FIG. 5. Lines of magnetic force; $R = 20$, $M = 1$, various R_m.

(b) Velocity along Axis

The value of the velocity on the axis $y = 0$ is a useful parameter for characterizing various features of the flow. The asymptotic behavior of this parameter for large x can be discussed analytically (see Sec. IV above), but here we present the information about this parameter obtained from the relaxation solution of the complete equations. In Fig. (1) we show the graphs of u as a function of x for various values of R for the hydrodynamic case ($M = 0$). To make clear the way in which the flow pattern can depend on the magnetic field, we also present Figs. 6 and 7. In the former we have taken $R = 20$, $M = 1$ and show $u(x, 0)$ as function of x for various values of R_m. In the latter we have fixed $R = 20$, $R_m = 10^{-4}$ and show the set of graphs of $u(x, 0)$ for various values of M.

(c) Behavior for Small x, y

It is found from the relaxation solution that in the immediate vicinity of $x = y = 0$, ψ can be represented very accurately by

$$\psi \approx y + \eta x^2 y, \tag{5.2}$$

where η is a constant. We tabulate below in Table V values of η corresponding to various values of R, R_m, M.

We see from the table that, for large R, η varies as $R^{-\frac{1}{2}}$. This is in accordance with boundary-layer theory, since the displacement thickness is proportional to $R^{-\frac{1}{2}}$, and so therefore also the correction to the potential flow.

However, the range of values of x for which our simple representation (5.2) holds is practically independent of R and is of length about 0.3. In terms of the variable x/R, which is the independent variable in the similarity solution of the boundary layer equations, this length tends to zero and u

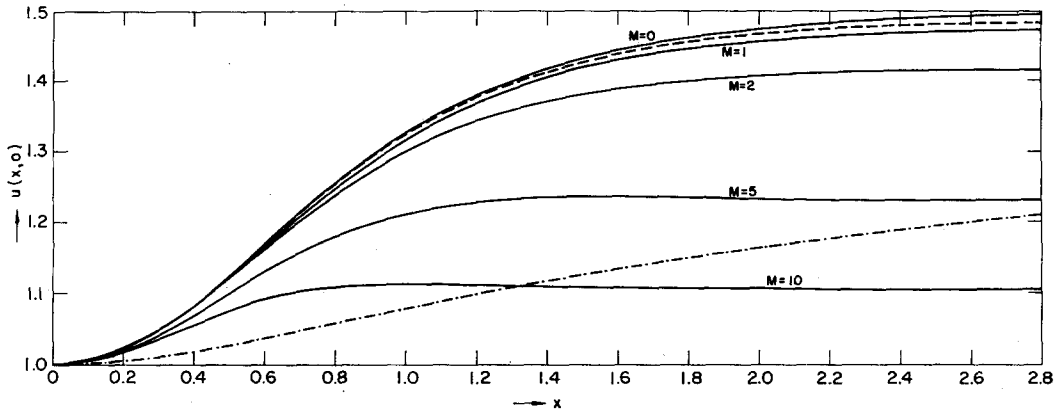

FIG. 6. Centerline velocity in magnetohydrodynamic case. Solid curves are for $R = 20$, $R_m = 10^{-4}$, and various values of M. The broken curve is for $R = 20$, $R_m = 50$, $M = 1$ (cf. Fig. 7). The dotted curve is for $R = 200$, $R_m = M = 1$.

in fact increases as $1 + (x/R)^{\frac{1}{2}}$ in the vicinity of $x = 0$ (see Fig. 1).

A similar study has been made of the behavior of the magnetic field for small x, y. It turns out that the transverse component is closely approximated by

$$B_2 \approx M - \tau R_m,$$

where τ depends on R, M alone. Values of τ as a function of M, R_m are given in Table VI.

(d) Pressure Drop

The pressure drop in the inlet region was computed by direct numerical integration of the equations of motion. In the absence of a magnetic field this is entirely straightforward. It is understood that, in the parabolic region, $\partial p/\partial y = 0$, $\partial p/\partial x = -6/R$. We have defined

$$q(y) = \lim_{x\to\infty} [p(0, y) - p(x, y) - (6x/R)], \qquad (5.3)$$

i.e., the excess pressure drop due to departure from parabolic flow in the inlet region. In Table VII we show $q(y)$ as a function of y, R for values of R from 20 to 500. We have also calculated the result of extrapolating to $R = \infty$. Boundary layer theory requires $q(y)$ to be independent of y and, indeed, our extrapolated values for $R \to \infty$ show a good approach to this situation. For comparison we have listed (Table I) some values obtained by other workers for large R. The situation for small R is shown in Table VIII. It should be noted that $q(y)$ is essentially the pressure distribution needed at the face $x = 0$ to maintain the input flow as specified. When the magnetic field differs from zero, the situation becomes more complex. We see from (2.1) that

$$\nabla[(p/\rho) - \phi] = \nu \nabla^2\mathbf{u} + \rho^{-1}\mathbf{J}\times\mathbf{B} - (\mathbf{u}\cdot\nabla)\mathbf{u}; \qquad (5.4)$$

ϕ is the potential of any external forces other than the magnetic field. It cannot in the nature of things be calculated apart from p, and we therefore drop the term from (5.4) and regard $p - \rho\phi$ as being the pressure. (Actually, similar considerations apply

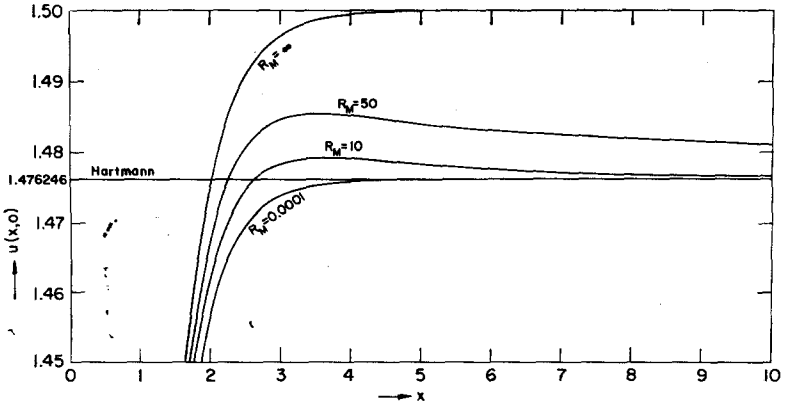

FIG. 7. Centerline velocities for $R = 20$, $M = 1$, and various R_m. The curve marked $R_m = \infty$ is for the case $M = 0$.

TABLE V. Coefficient in expansion of ψ for small x, $y[\psi = y + \eta x^2 y]$.

R	M	R_m	η	$\eta R^{\frac{1}{2}}$
0	0		2.07	
0.5	0		2.01	1.42
5	0		1.43	3.20
20	0		0.538	2.41
50	0		0.288	2.04
100	0		0.189	1.89
200	0		0.126	1.78
500	0		0.077	1.72
∞	0			1.70
(extrapolated)				
20	0		0.538	
20	1	0.0001	0.522	
20	5	0.0001	0.48	
200	0		0.126	
200	1	1	0.12	
20	1	0.0001	0.522	
20	1	1	0.530	
20	1	50	0.538	

in the hydrodynamic case, and we have tacitly assumed them.) A more serious difficulty, specific to this case, arises from the fact that our relaxation solutions for ψ, β does not give us all the information required for the integration of the vector equation (5.4). The first two components of this set can be written (in the dimensionless variables, and with $p - \rho\phi$ replaced by p)

$$\partial p/\partial x = 2R^{-1}(\nabla^2 u + J_2 B_3 - J_3 B_2) - [u(\partial u/\partial x) + v(\partial u/\partial y)], \quad (5.5)$$

$$\partial p/\partial y = 2R^{-1}(\nabla^2 v + J_3 B_1 - J_1 B_3) - [u(\partial v/\partial x) + v(\partial v/\partial y)]. \quad (5.6)$$

To make the problem definite we assume that the boundary conditions are such as to ensure that $J_1 = J_2 = 0$ throughout the field. Since none of the variables depend on z it follows from (2.3) that J_1 and J_2 will both vanish everywhere provided that $\partial B_3/\partial x = \partial B_3/\partial y = 0$, i.e., B_3 is constant. We may remark that, in terms of our dimensionless variables, $J_3 = (-2/R_m)\nabla^2\beta$ and is in fact determinable from the relaxation solution.

TABLE VI. Change in magnetic field in immediate vicinity of inlet for small R_m : $B_2 \approx M - \tau R_m$.

R	M	τ
20	0	0.000
20	1	0.041
20	2	0.079
20	5	0.157
20	10	0.214
200	1	0.014

TABLE VII. Excess pressure drop $q(y)$ as a function of y and R (no magnetic field).

y	R					
	20	50	100	200	500	∞ (extrapolated)
0.0	0.1180	0.2273	0.2632	0.2875	0.3077	0.3243
0.1	0.1225	0.2298	0.2650	0.2887	0.3083	0.3244
0.2	0.1364	0.2373	0.2704	0.2922	0.3103	0.3252
0.3	0.1615	0.2517	0.2799	0.2983	0.3135	0.3260
0.4	0.2016	0.2716	0.2944	0.3079	0.3183	0.3266
0.5	0.2627	0.3033	0.3159	0.3211	0.3251	0.3284
0.6	0.3580	0.3507	0.3477	0.3420	0.3369	0.3327
0.7	0.524	0.431	0.399	0.374	0.356	0.344
0.8	0.868	0.563	0.493	0.434	0.389	0.353
0.9	1.918	1.010	0.737	0.589	0.474	0.381

We note that for large x, when the Hartmann flow is fully established,

$$\partial p/\partial x \sim -(2KM/R)\sinh M = P_1 \quad \text{(say)}, \quad (5.7)$$

$$\partial p/\partial y = (\partial/\partial y)[-(R_m K^2/2R) \cdot (\sinh My - y\sinh M)^2]. \quad (5.8)$$

If now we define

$$q_m(y) = \lim_{x\to\infty}[p(0, y) - p(x, y) + P_1 x], \quad (5.9)$$

it can easily be seen that it goes over to $q(y)$ in the limit of small M. In Table IX we show $q_m(y)$ as function of y for $R = 20$, $R_m = 0.0001$, and various values of M; and also for a range of R_m with $M = 1$.

(e) Distance to Termal Regime

We define x_∞ as the smallest value of x for which

$$[u(\infty, 0) - u(x, 0)] = 0.03[u(\infty, 0) - u(0, 0)]. \quad (5.10)$$

TABLE VIII. Excess pressure drop (times R) for small Reynolds numbers (no magnetic field).

y	R			
	0	0.5	5	20
0.0	−4.86	−4.56	−2.59	2.36
0.1	−4.74	−4.45	−2.51	2.45
0.2	−4.38	−4.11	−2.24	2.73
0.3	−3.74	−3.50	−1.79	3.63
0.4	−2.74	−2.49	−1.12	4.03
0.5	−1.24	−1.16	−0.06	5.25
0.6	1.04	1.07	1.83	7.16
0.7	4.75	4.76	5.28	10.48
0.8	12.1	12.1	12.4	17.36
0.9	33.9	33.9	33.9	38.36
0.95	77	77	77	81

TABLE IX. Excess pressure drop $q(y)$ in inlet region for various R, R_m, M as function of y.

R	200	200	20	20	20	20	20	20	20
R_m	1		50	10	1	0.0001	0.0001	0.0001	
y	M								
	1	0	1	1	1	1	2	5	0
0	0.266	0.287	−0.23	0.028	0.090	0.091	0.029	−0.13	0.1180
0.1	0.268	0.289	−0.22	0.033	0.095	0.096	0.034	−0.13	0.1225
0.2	0.271	0.292	−0.20	0.049	0.108	0.111	0.049	−0.13	0.1364
0.3	0.278	0.298	−0.16	0.077	0.133	0.137	0.072	−0.11	0.1615
0.4	0.288	0.308	−0.10	0.120	0.174	0.178	0.112	−0.07	0.2016
0.5	0.301	0.321	−0.027	0.187	0.236	0.243	0.174	−0.01	0.2627
0.6	0.323	0.342	0.082	0.29	0.34	0.34	0.27	0.09	0.3580
0.7	0.356	0.374	0.26	0.48	0.52	0.52	0.44	0.26	0.524
0.8	0.414	0.434	0.66	0.86	0.90	0.91	0.8	0.6	0.868
0.9	0.581	0.590	1.7	2.1	2.1	2.1	2.0	1.8	1.918

We have described elsewhere[2] the nature of the dependence of x_∞ on R in the absence of a magnetic field. For the sake of completeness we include the results below in Table II, along with those for the magnetohydrodynamic problem, comparing them in Table X, with results obtained for large R by other workers. These results are also of importance for checking the accuracy of the solution because of their close relation with the coefficient α_1 featuring in (4.1).

It should be noted that for $R_m \gg 1$ the flow can still vary considerably even for x greater than the value of x_∞ given by (5.10) (cf. Fig. 7).

(f) Growth of Boundary Layer

We define the boundary layer as the region near the solid boundary in which $u(x, y) < 0.9\, u(x, 0)$. It is clear, that for large x, the growth of this boundary layer will be materially affected by the opposite wall, but there is some interest in studying the rate of growth for small and moderate x.

Denoting the thickness of the boundary layer at either one of the walls by $\delta(x)$, we plotted $\log \delta(x)$ against $\log x$ and found that, for the initial values of x, the points lay on a straight line. The slope of this line, λ (say), depends on the physical parameters and we give below, in Table XI, values of λ as a function of R, for the hydrodynamic case $M = 0$.

TABLE X. Distance to the point x_∞ where terminal régime is 97% established: result for large R ($M = 0$), compared with results obtained by other workers.

x_∞/R	Author
0.0800	Schlichting
0.0844	Hwang and Fan
0.0880	Bodoia and Osterle
0.0884	Extrapolation from Table II
0.0908	Roidt and Cess
0.0965	Snyder

(g) The Magnetic Field

The development of the Hartmann magnetic field in the inlet region has also been calculated. Defining

$$\Delta\beta(x) = \beta(x, 0) - \beta(x, 1) = \beta(x, 0) + Mx, \quad (5.11)$$

we present in Fig. 8 curves which show the development of $\Delta\beta(x)$ and its dependence on the physical parameters. In Fig. 5 we show typical lines of magnetic force for various cases.

We note incidentally that for a perfectly conducting fluid ($R_m \to \infty$) the flow in the inlet region (outside of the magnetic boundary layer) reverts to the hydrodynamic pattern, while the magnetic lines of force travel with the stream. In this connection we draw attention to Fig. 7 and to the broken curve in Fig. 6.

TABLE XI. Growth of boundary layer, proportional to x^α. Depencence of α on R.

R	α
0	1.2
5	1.1
20	0.94
50	0.81
100	0.73
200	0.68
500	0.59
∞ (extrapolated)	0.49

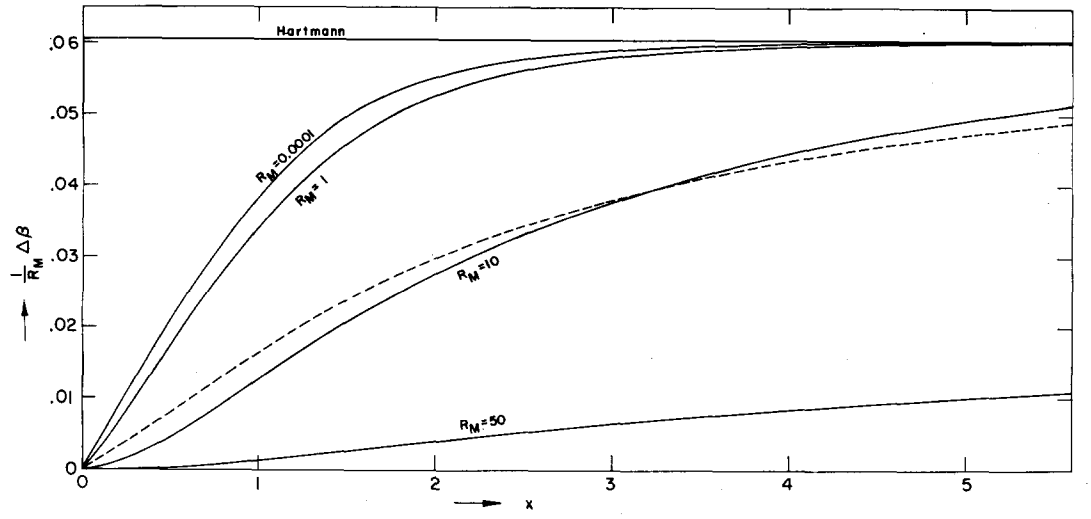

FIG. 8. Development of z component of magnetic vector potential on centerline; $\Delta\beta = \beta(x, 0) + Mx$. Curves are for $R = 20$, $M = 1$, and various R_m. The broken curve is for the case $R = 200$, $R_m = M = 1$.

We might mention that previous workers on this problem have neglected the change induced in the magnetic field by the flow. This is valid for $R_m \ll 1$, but certainly not otherwise.

VI. WANG AND LONGWELL'S SOLUTION

We are grateful to a referee who has drawn our attention to an interesting paper by Wang and Longwell.[10] Using a notation slightly different from ours, these authors have solved a case of the hydrodynamic problem (in our notation, the case $M = 0$, $R = 140$). The complete equations were solved without any approximations, though the numerical procedure differs from ours. They have reduced the fourth-order differential equation to a pair of second-order differential equations by introducing the vorticity ω and the additional equation

$$\omega = -\nabla^2\psi. \tag{6.1}$$

The difficulty of locating x_∞ was circumvented by a change of coordinates

$$\eta = 1 - (1 + cx)^{-i} \tag{6.2}$$

in which c is a positive constant. The actual finite difference formulation is that applied by Allen and Southwell[11] to a different problem and is rather more sophisticated than ours. Although they worked on a considerably coarser grid than that used in this paper, their results are in substantial agreement with ours. In particular, they too obtained, for small values of x, velocity profiles very similar to those shown in Figs. 2, 3.

Defining the inlet length L as the distance from the entrance at which the center line velocity achieves 98% of its asymptotic value, they find that, in our notation,

$$L \sim 0.067\, R. \tag{6.3}$$

Tables of velocity components obtained by us[2] suggest that 0.07 might be a more accurate value. Since $d\eta/dx$ tends to zero with increasing x, a quite small discrepancy in η will lead to a relatively large change in x. This may well be the source of the discrepancy.

We should also mention that Wang and Longwell dealt with another physical case, in addition to that already mentioned, viz., that of a channel from $x = -\infty$ to ∞, but with the same conditions as ours imposed at $x + 0$.

VII. CONCLUSION

We mention in conclusion that more complete numerical results for the special case $M = 0$ have been tabulated elsewhere (Ref. 2). All of the numerical work reported here was executed on the Control Data 1604A computing machine at the Weizmann Institute of Science.

ACKNOWLEDGMENT

The research reported in this paper has been supported by the Office of Scientific Research under Grant AF EOAR 63-73 through the European Office of Aerospace Research, United States Air Force.

[10] U. L. Wang and P. A. Longwell, J. Am. Inst. Chem. Engrs. 10, 323 (1964).
[11] D. N. de G. Allen and R. V. Southwell, Quart. J. Mech. Appl. Math. 8, 129 (1955).